AC/TiO2 granular photocatalysts optical properties: Material composition effect on the radiative transfer in a photoreactor

Enrique Ribeiro, Gaël Plantard, J.-F. Cornet, F. Gros, C. Caliot, Vincent Goetz

AC/TiO_2 granular photocatalysts optical properties: material composition effect on the radiative transfer in a photoreactor

E. Ribeiro[(*,1,2)], G. Plantard[(1,2)],J.-F. Cornet[(3)] , F. Gros[(3)] , C. Caliot[(4)] , and V. Goetz[(1)]

[(1)]PROMES CNRS, UPR 8521, Rambla de la thermodynamique 66100 Perpignan, France.
[(2)]University of Perpignan Via Domitia, 52 Paul Alduy 66100 Perpignan, France.
[(3)] University of Clermont Auvergne, Clermont Auvergne INP, CNRS, Institut Pascal, F-63000 Clermont–Ferrand, France.
[(4)] Laboratory of Mathematics and its Applications, University of Pau, E2S UPPA, CNRS, LMAP, Allée du parc Montaury, 64600 Anglet, France.

* Corresponding author. Tel.: +33602311658

E-mail address: enrique.ribeiro@promes.cnrs.fr

Abstract:

The radiative transfer analysis in photoreactor with heterogeneous media is still a challenge for reasons relative to solid particles structural complexity or materials complex optical properties. This article aims to study the radiative transfer in a photoreactor containing Activated-Carbon/Titanium Dioxide (AC/TiO_2) composite particulate media. A focus was made on the analysis of the photon rate absorbed by these media, which is a key value for the further study of chemical photo-reaction for which they are intended into the system. The radiative properties of these media were first consistently defined using different mixing laws for refractive index calculation, coupled to Mie theory. A validation of the radiative properties was achieved by solving the radiative transfer equation using a Monte Carlo algorithm and by comparing the results of transmittance modelling of each media with transmittance experiments. The second part of the work consisted in the use of a second Monte Carlo algorithm for modelling local radiant energy repartition in the studied photoreactor and access the rate of energy absorbed. These parameters are some key tools for the description and the assessment of reactions in a defined photoreactor. An originality of the study comes from the wide range of AC/TiO_2 composition studied through the work which allows to analyze the evolution of the radiative properties, radiant energy repartition and rate of energy absorbed as a function of the AC/TiO_2 material composition.

Keywords : *Photoreactor ; Radiative transfer analysis ; suspended media ; composites ; mixing laws ; optical bench*

Nomenclature

Acronyms :

AC	Activated Carbon
BM	Bruggeman Mixing
MC	Calculated through Monte-Carlo algorithm
MG	Maxwell Garnett
PMMA	PolyMethylMethAcrylate
TiO_2	Titanium Dioxide
RTE	Radiative Transfer Equation
VA	Volume Averaging method
x_AC/TiO_2	Composite sample at x volume fraction of Activated Carbon

Symbols :

$<A_\lambda>$	Total Rate of Radiant Energy Absorbed ($W.m^{-3}.nm^{-1}$)
C_{susp}	Suspension concentration ($kg.m^{-3}$)
D	Particle diameter (µm)
E_{abs}, E_{sca}, E_{ext}	Specific absorption, scattering and extinction coefficients ($m^2.kg^{-1}$)
f_v	Volume ratio of particles in the water media (m^3/m^3)
G_λ	Local available radiant energy ($W.m^{-2}.nm^{-1}$)
k_{abs}, k_{sca}, k_{ext}	Absorption, scattering and extinction coefficients (m^{-1})
L	Medium total thickness (m)
n(D)	Volumetric particle size distribution ($\mu m^{-1}.m^{-3}$)
N_T	Total number of particles per unit volume (m^{-3})
$p_\lambda(\vec{\Omega}, \vec{\Omega}')$	Phase function depend on the direction $\vec{\Omega}$
Q_{ext}, Q_{sca}, Q_{abs}, Q_{back}	Extinction, scattering, absorption and backscattering efficiencies (-)
r	Volumetric reaction rate ($kg.m^{-3}.s^{-1}$)
V_P	Particle volume (m^3)
$\hat{\varepsilon}_\lambda$	Effective complex permittivity (-)
α	ratio of the specific absorption coefficient on specific extinction coefficient (-)
θ	Polar angle (rad)
κ	Imaginary part of the refractive index (-)
µ	Mean size distribution value (µm)
ρ	Density material ($kg.m^{-3}$)
σ	Standard deviation (µm)
τ	Length variable used in Monte-Carlo algorithm (m)
φ	Azimuthal angle (rad)
Φ	Radiant energy flux ($W.\ m^{-2}$)
Ω	Solid angle (sr)

Indices :

0	Relative to incident/initial
Exp	Relative to experimental data
Mix	Relative to the effective mixture of components
T	Relative to the transmitted flux
λ	Relative to the wavelength λ

Introduction

Photoreactors have received increasing attention due to their potential uses in environmental applications such as water treatment [1-5], but more recently for fuel production such as water photoelectrochemistry [6-7] and CO_2 photoreduction [8,9]. Photoreactors are devices that allow the efficient contacting of photons and reactants with the photocatalyst. They differ significantly from other chemical reactors, not only in their geometries, but also in the importance given to the collection and efficient distribution of light. The absorption of radiation allows the generation of charges (electron/hole pairs) to produce radicals via an interface that is the photo-catalyst. These radicals can be used for the photodegradation of species or for the photo-conversion of molecules (H_2O or CO_2) [10,11]. Among the various configurations and options available, there is increasing interest in using suspended solids capable of catalyzing photoreactions in the gas or liquid phase, thus avoiding the need to add reagents [12,13]. These heterogeneous photocatalytic processes are of increasing interest to industry, but there are still impasses to be addressed [14] regarding how phase heterogeneities make it more difficult to predict and control light harvesting in heterogeneous photoreactors compared to homogeneous photoreactors.

To address this challenge, which involves the description of the local radiant energy available in heterogeneous photoreactors [14-18], the rich literature proposes studies on different reactor configurations and types of photocatalysts depending on the targeted applications. Among the different approaches and models studied, the Monte Carlo model emerges as a descriptive and perfectly adapted approach to predict the local radiant energy in different photoreactor geometries [19]. It consists in solving the radiative transfer equation (RTE) via a stochastic approach, following a statistically suitable number of photons from the radiant energy source to the absorption in the medium or the loss in the reactor walls. This approach is relevant for the description of RTE in scattering reaction media such as monodisperse suspensions of commonly studied photocatalysts like TiO_2, ZnO and CuO in water [20-21]. Subsequently, this method was consolidated and applied to the prediction of the radiative properties of polydisperse spherical particle suspensions [22,23]. In general, the studies remain numerous and concern the large panel of catalysts available for environmental applications (TiO_2, ZnO) or fuel production such as Cds. TiO_2 is the most widely studied candidate as it presents characteristics (inert, non-soluble and non-toxic) that facilitate its use and handling, in particular for water treatment applications. It should be noted that very few studies have been carried out on complex photocatalytic media such as composite powders made of several elements or

supported photocatalytic materials such as cellular foams. Their peculiarities regarding both their shaping and their optical properties turn complex their radiative properties calculation.

The literature ranks oxidation processes as a promising technology for solar applications [2]. Use of the solar resource entails careful management of its specific resource characteristics, such as its distribution of spectral density and disparity in its geographical distribution but above all its fluctuating nature due alternating daily and seasonal cycles but also to intermittent weather conditions (cloud, rain, strong sunshine) [24-26]. Solar-based systems therefore need a storage solution that works during night-time or low-sunlight periods or during pollution peaks in order to be able to concentrate the pollution on smaller volumes. In this context, recent advances in photocatalysis have highlighted the value of associating several materials in the form of particulate composites with the aim of optimizing photocatalytic performances [27-29] or coupling synergistic properties such as adsorption with photo-oxidation for water treatment applications [30]. Adsorbent materials offer a solution for managing intermittency by making it possible to store a wide range of molecules [31-33]. Specifically, coupling activated carbon (AC) with TiO_2 in various forms has emerged as a promising solution for water treatment applications [30], as the coupled composite systems can enhance pollutant removal from water by using the complementary functions of adsorption and photo-oxidation [33,34]. These composites therefore combine a catalyst capable of using solar radiation to produce radicals, and an adsorbent material capable of filtering and concentrating the pollution during periods of no sunlight. Many forms of AC/TiO_2 composites have been studied [35,36] and used in laboratory photoreactors for chemical engineering investigations [30]. However, despite the promise of these materials for photoreactor-based water treatment applications, no study yet has focused on their optical properties and their effects on radiative transfer when they are used in photoreactors. This information is a vital input to establish the reaction rate law that depends on the number of locally available photons [17], which is a bottleneck for efforts to describe the local volumetric rate of radiant energy absorbed (LVREA) at each point of the photoreactor. LVREA needs to be known in order to rigorously study the photochemical reactions occurring in the system [14].

For this study, the goal is to establish the photon density profiles available locally in the photoreactor to describe and optimize the photoreaction rates governing the transformation process. Here, the originality is to work with granular composites presenting optical specificities and characteristics relevant for a solar application. These are AC/TiO_2 granular composites prepared through a mechano-synthesis process based on a simple and robust one-step protocol [32]. In contrast to the literature, this method allows the design of composites

covering a wide range of composition, with all other characteristics preserved. To meet the challenge, the paper proceeds in four steps. A first section is dedicated to the presentation of the materials and their characteristics, as well as the description of the experimental optical bench used. Then, the approach and the theoretical considerations necessary for the RTE are developed, which is followed by the validation of a mixing law allowing the closest theoretical prediction of the radiative properties. Finally, the last part details the main results. First, the study of the local available radiant energy in suspensions of AC/TiO_2 composites of varying composition is presented. The interest of such a composite in a photoreactor for an optimal use of the radiation in relation with the problem of the management of the solar resource is discussed. To this end, absorbed radiant energy profiles are established to understand and describe the photo-oxidation capabilities in a photoreactor.

1. Experimental part

1.1 AC/TiO_2 materials characteristics

A compositionally-varied set of AC/TiO_2 composite powders that we had previously successfully prepared [32] from commercial Aeroperl® P25/20 TiO_2 and Picahydro S23 AC was used here for the purposes of this work. These powders were shown to be composed of spherical AC/TiO_2 aggregates, which thus meet the particle shape assumption of the Mie solution for predicting radiative properties. Five compositionally-distinct AC/TiO_2 composites were selected, named 6_AC/TiO_2, 26_AC/TiO_2, 54_AC/TiO_2, 74_AC/TiO_2 and 95_AC/TiO_2 in reference to their percent volume of AC. These AC/TiO_2 powder aggregates were all prepared from the same one-step one-pot mechanosynthesis protocol with well-characterized composition and size distribution, and all were homogeneous on both these characteristics [32]. Indeed, the particle-size distributions of these materials were well fitted by a Gaussian function defined as (Equation 1):

$$n(D) = \frac{\frac{1}{\sigma\sqrt{2\pi}} e^{-\frac{1}{2}\left(\frac{D-\mu}{\sigma}\right)^2}}{\frac{1}{6}\pi D^3} \qquad \text{(Equation 1)}$$

where D is particle diameter (m), μ is mean size distribution value (m), and σ is the standard deviation (m). For each composite, Table 1 reports the characteristics required for Mie-based

prediction of their radiative properties, i.e. (i) the two Gaussian parameters that serve to describe their previously characterized Gaussian particle-size distributions and (ii) their respective densities. Table 1 gives the mean particle diameter of both the AC particles and the TiO_2 particles that make up the above-mentioned AC/TiO_2 composites.

	Gaussian granulometry parameters			
Materials	**Distribution mean μ (μm)**	**Standard deviation (μm)**	**Determination coefficient R^2**	**Material density ρ ($g.cm^{-3}$)**
Raw TiO_2	41.00	17.24	0.98	3.95
6_AC/TiO_2	3.16	1.05	0.99	3.70
26_AC/TiO_2	2.79	1.00	0.97	2.94
54_AC/TiO_2	3.25	1.06	0.99	1.94
74_AC/TiO_2	3.47	0.85	0.97	1.29
95_AC/TiO_2	2.90	1.04	0.99	0.64
Raw AC	496.54	55.12	0.98	0.60

Table 1. *Granulometry Gaussian function parameters of each composite and raw materials powders and their respective density* [35].

A digital image processing protocol for optical granulometry developed in previous work [35] uses SEM images to enable size-based discrimination of the powder samples under study. This approach was applied for characterizing the particle-size distribution of the AC/TiO2 composite powders.

1.2. Optical bench characteristics and protocol

An optical bench successfully set up in our previous work was used here to experimentally assess the transmittance of particulate media in suspension form [23].

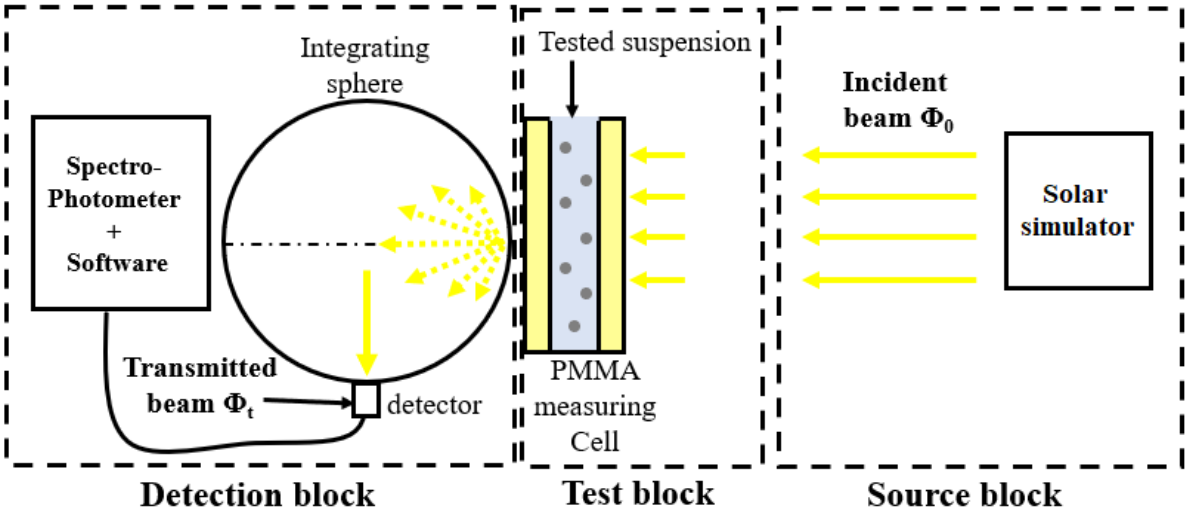

Figure 1. *Schematic of the optical bench set up blocks for particle suspension experimental assessment of the transmittance*

As shown by the simple scheme given in Figure 1, the set-up used to measure transmittance is composed of three blocks: (i) the source block, which comprises a solar spectrum-like collimated source (1000 W) uniformly irradiating the whole surface of the measuring cell; (ii) the test block, composed of the tested suspension container, which is a 0.02 m-thick parallelepiped-shape measuring cell featuring a UV-transparent polymethyl methacrylate (90% UV transmission) plate and a magnetic stirrer used to keep the tested suspension constantly homogeneous; (iii) the detection block, composed of a 7 cm²-aperture integrating sphere coupled to a high-res Ocean Optics HR4000 spectrophotometer (detector range: 250–1100 nm).

The role of the detection block was to collect and integrate both direct and diffuse radiant energy transmitted through the test block where multiple scattering events can occur depending on the optical properties of the tested suspension. The software-controlled acquisition settings were fixed at a detection range of 350–500 nm and a total acquisition time set at 5 seconds comprising 25 analyses of 200 ms each to ensure representativity and repeatability of the measurement. The latter requires two preliminary steps: (i) registration of the ambient radiant noise, which can then be removed from the measure, and (ii) registration of the reference incident signal $\Phi_{0,exp}$, which is acquired placing the measuring cell containing only water between the source and the detection block. The water is then immediately replaced by the tested suspension and a transmittance measurement is done. Note that here, the transmittance measurement, called $\Phi_{t,exp}$, is a relative one, and is normalized between 0 and 1 by ratioing the absolute transmittance value given by the detection block to the $\Phi_{0,exp}$ reference.

2. Theoretical approach

2.1. RTE formulation and Monte Carlo modeling

Two previously-established one-dimensional Monte Carlo method (MCM) algorithms [23] were used in this work with the aim of determining the transmitted photon fluxes (transmittances, T_λ) and locally available photon fluxes within the photoreactor. The first algorithm, named MCM1, aims to predict the amount of light transmitted through the polymethyl methacrylate measuring cell containing a tested suspension whose radiative properties need to be defined. These results are then compared against measurements made on an optical bench in order to validate our approach. The second algorithm, named MCM2, aims to assess, for a chosen wavelength λ, the one-dimensional variation in local available radiant energy G_λ ($W.m^{-2}.nm^{-1}$) along the medium travelled thickness x of the tested suspension, which needs to be known in order to investigate the radiative transfer in this kind of particulate system. This quantity can then be used to describe the light attenuation profile in a photoreactor, and its value is discussed in the last section of the paper. Here we provide a brief description of the MCMs employed in Figure 2. An exhaustive description of these algorithms can be found in our previous work [23].

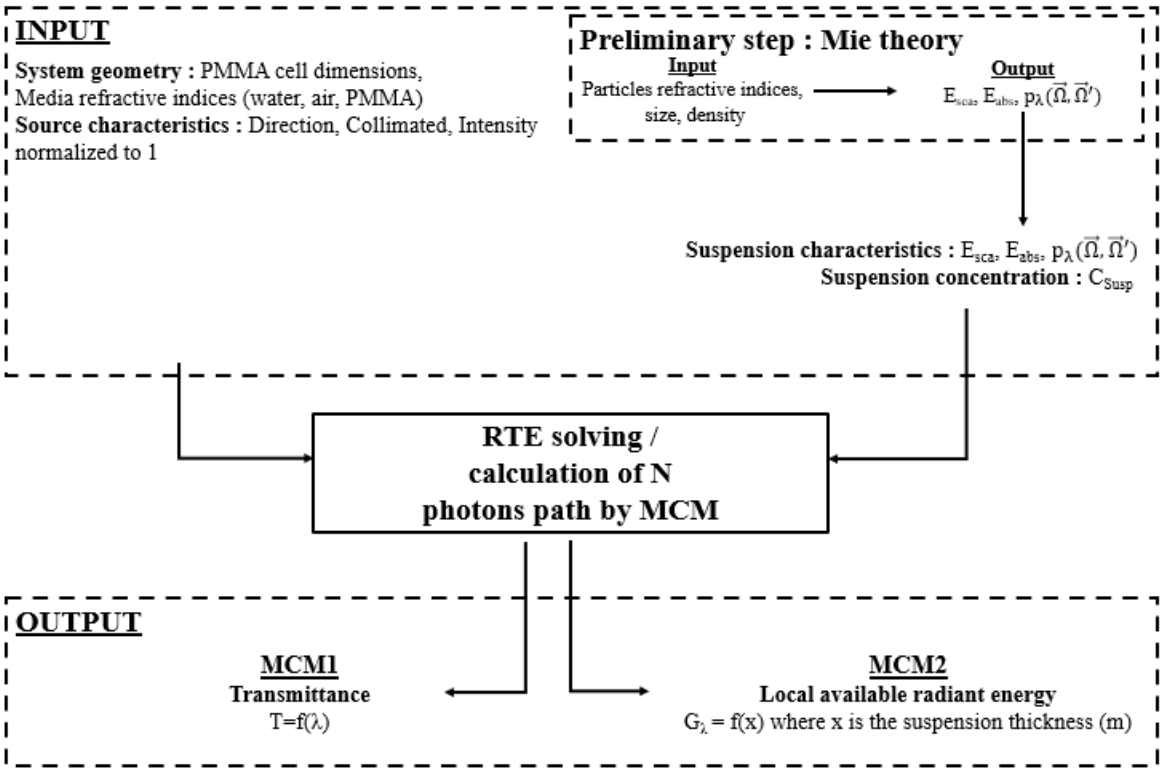

Figure 2. *Description of the input necessary for two previously established MCM allowing the RTE solvation for transmittance (MCM1) or Local available radiant energy (MCM2) predictions.*

2.2. Mie-based prediction of radiative properties

As shown in Figure 2, the resolution of the radiative transfer equation using MCM requires defined radiative properties of the tested particulate media, i.e. its angle-dependent scattering function $p_\lambda(\vec{\Omega},\vec{\Omega}')$, and the specific extinction, scattering and absorption coefficients, which are noted E_{ext}, E_{sca} and E_{abs}., respectively. For particulate media, if the particles in suspension can be assimilated to spheres, then the media's radiative properties can be calculated thanks to the work of Lorenz-Mie, who solved Maxwell's equations for the scattering of a plane wave by a single sphere [21]. The Mie solution takes the form of an infinite series that requires a computation of the spherical Riccati–Bessel functions. This theoretical approach was done by Bohren & Huffman [37] who demonstrated rigorous calculation of the intrinsic radiative properties of a single particle ($p_\lambda(\vec{\Omega},\vec{\Omega}')$ Q_{ext}, Q_{sca}, and Q_{abs}) thanks to their well-known BHMIE program. As shown in many works, the BHMIE program can compute the radiative properties of a polydispersion by implementing the following integrals (Equations 2-4) [22] :

$$N_T = \frac{f_v}{V_P} = \int_0^\infty n(D)dD \qquad \text{(Equation 2)}$$

$$E_{abs/sca/ext,\lambda} = \frac{\pi}{4}\frac{\int_0^\infty D^2 Q_{abs/sca/ext,\lambda} n(D)dD}{C_{susp}} \qquad \text{(Equation 3)}$$

$$p_\lambda(\vec{\Omega},\vec{\Omega}') = \frac{\int_0^\infty D^2 Q_{sca,\lambda} p(D,\vec{\Omega},\vec{\Omega}') n(D)dD}{\int_0^\infty D^2 Q_{sca,\lambda} n(D)dD} \qquad \text{(Equation 4)}$$

where N_T is total number of particles per unit volume (m^{-3}), f_v is volume ratio of particles in the water media (m_{sol}^3/m_{liq}^3), V_P is the mean particles volume (m^3) and $n(D)$ is the volumetric particle size distribution function, C_{susp} is concentration of suspension ($kg.m^{-3}$), Q_{ext}, Q_{sca}, Q_{abs}, Q_{back} are the extinction, scattering, absorption and backscattering efficiencies and $E_{abs,\lambda}, E_{sca,\lambda}, E_{ext,\lambda}$ are the specific absorption, scattering, and extinction coefficients ($m^2.kg^{-1}$), respectively. The phase function $p_\lambda(\vec{\Omega},\vec{\Omega}')$ depends on direction $\vec{\Omega}$ which is defined by the solid angle Ω composed of the polar angle θ and the azimuthal angle ϕ. Note that for spherical particles, the phase function presents a symmetry that means its normalization can be expressed independently of the azimuthal angle (Equation 5):

$$\frac{1}{4\pi}\iint_{4\pi} p_\lambda(\vec{\Omega},\vec{\Omega}')d\Omega = \frac{1}{4\pi}\int_0^{2\pi}\int_0^{\pi} p_\lambda(\theta,\phi,\theta',\phi')\sin\theta d\theta d\phi$$

$$= \frac{1}{2}\int_0^{\pi} p_\lambda(\theta,\theta')\sin\theta d\theta = 1 \qquad \text{(Equation 5)}$$

The scattering function of the studied particles will thus be presented in the form $p_\lambda(\theta,\theta')$ normalized to 4π steradians in this work, as it is usual in radiative transfer studies.

From a practicality point of view, this BHMIE program requires few input parameters: particle diameter D or particle size distribution n(D) in a polydispersion setting, plus the material density ρ and its complex refractive index $m_\lambda = n_\lambda - i\kappa_\lambda$ in which the real part corresponds to the refractive index n_λ and the imaginary part to the attenuation index κ_λ.

2.3 Formulation of the complex refractive index mixing laws

An approximation of the effective complex refractive index is needed in order to define refractive indices for multicomponent particles like composite aggregates [38]. In the literature, there are various different laws for defining the effective complex permittivity $\hat{\varepsilon}_\lambda$ of a media, which is directly linked to the complex refractive index m_λ through the simple relation $m_\lambda = \sqrt{\hat{\varepsilon}_\lambda}$. These laws cover different theoretical arrangements of binary composite materials in a simple way and have been successfully employed to compute effective medium complex permittivity in particular cases [39]. However, these laws have shown limitations for describing complex mixtures, where it has not always led to correct results [38].

The particles studied in this paper are composed of several components with distinct optical properties. The constituents (AC and TiO_2) form aggregates whose entities are homogeneously distributed in the volume of the particle. Therefore, two mixing laws proposed and studied in the literature to describe such mixtures were used; *i.e.* Bruggeman Mixing (BM) and a simple Volume Averaging (VA) one, which really differ each other from their approach of the effective medium mixing rule problem. Indeed, BM formula considers the mixture as spherical inclusions in a homogeneous background medium (Figure 3.A), while VA is an ideal binary mixture approach for which both components are unmixed in the effective medium volume (Figure 3.B). They were compared in order to evaluate the most relevant one to represent the CA/TiO_2 composite particles.

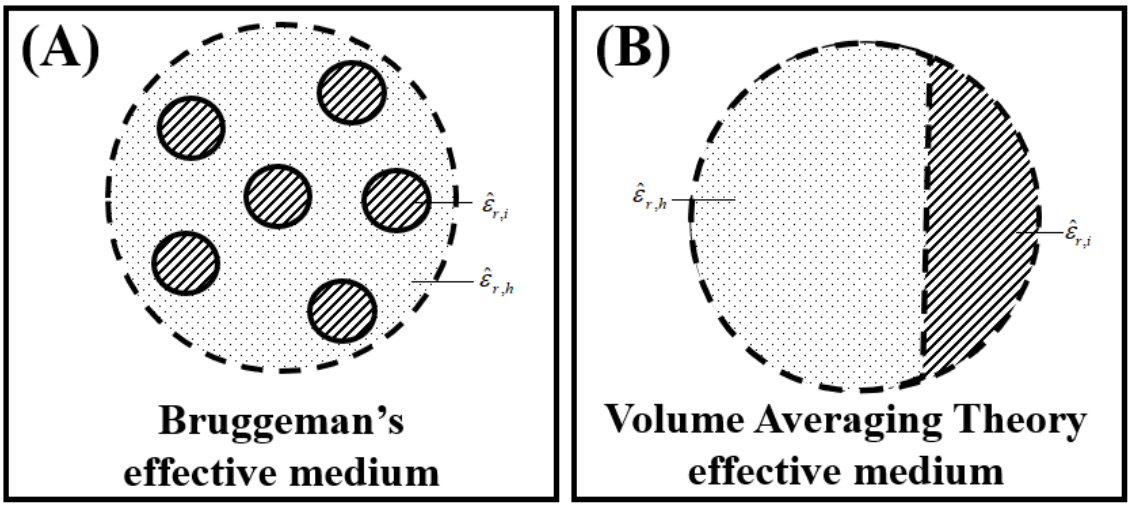

Figure 3. *Schematic effective medium binary spatial structuration from BM (A) and VA (B) laws points of views. The effective medium is represented by the dashed circles, the inclusion is represented by hatched circles and the matrix by dotted-filled circles.*

2.3.1. Bruggeman mixing law

In 1904, Maxwell Garnett (MG) proposed a theory for the approximation of the effective complex permittivity of a medium composed of two different compounds [40]. The MG formula computes the complex permittivity of an effective medium using the volume fractions of its two individual components, i.e. the host and the inclusion. However, it frequently proved inapplicable in cases where medium and inclusion share comparable volume fractions [38]. In 1935, Bruggeman (BM) [41] proposed a law derived from the original MG formula that is symmetrical with respect to each medium component and thus does not treat them differently. Bruggeman's law thus brings a correction to the MG formula under conditions when the volume fraction of inclusions is not very small. BM's law can thus serve to compute the complex permittivity of an effective medium using the volume fraction of the individual component, following Equation 6:

$$f_i \frac{\hat{\varepsilon}_{r,i} - \bar{\hat{\varepsilon}}_{r,mix}}{\hat{\varepsilon}_{r,i} + 2\bar{\hat{\varepsilon}}_{r,mix}} + (1 - f_i) \frac{\hat{\varepsilon}_{r,h} - \bar{\hat{\varepsilon}}_{r,mix}}{\hat{\varepsilon}_{r,h} + 2\bar{\hat{\varepsilon}}_{r,mix}} = 0 \qquad \text{(Equation 6)}$$

where $\bar{\hat{\varepsilon}}_{r,mix}$ is the effective complex permittivity of the mixed material, $\hat{\varepsilon}_{r,i}$ is complex permittivity of the inclusion, $\hat{\varepsilon}_{r,h}$ is complex permittivity of the host medium, and f_i is volume fraction of the inclusion.

2.3.2. Volume averaging method

Several empirical simple mixing laws have been established, mainly for predicting the effective complex permittivity of liquid binary mixtures [42]. One of the simplest and most effective of these laws is a volume averaging one (VA) [39], which derived from the application of the volume averaging method to the Maxwell equations and can be expressed through the relation (Equation 7) :

$$\bar{\hat{\varepsilon}}_{r,mix} = f_i \hat{\varepsilon}_{r,i} + (1 - f_i)\hat{\varepsilon}_{r,h} \quad \text{(Equation 7)}$$

3. Results and discussion

First, we checked the validity of the radiative properties found for AC and TiO_2 using a comparative method presented in Text S1. This step provided confidence on the calculated radiative properties of the raw materials before integrating them in the mixing laws.

3.1. Comparison and validation of the mixing laws

The VA and BM laws were used to calculate the effective complex refractive index of each composite under study. There was less than 5% difference between results from the two mixing laws, as seen in the complex refractive index values for the composite reported in Table 2.

	Complex refractive index m = n – iκ at different wavelengths λ (nm)			
Materials	**λ = 350 nm**	**λ = 400 nm**	**λ = 450 nm**	**λ = 500 nm**
AC	1.503 – 0.011 i	1.497 – 0.014 i	1.487 – 0.017 i	1.478 – 0.020 i
TiO_2	2.930 – 0.175 i	2.589 – 0.018 i	2.509	2.429
1_AC/TiO_2	2.887 – 0.170 i (BM) 2.887 – 0.170 i (VAT)	2.556 – 0.018 i (BM) 2.556 – 0.018 i (VAT)	2.478 – 0.001 i (BM) 2.479 – 0.001 i (VAT)	2.400 – 0.001 i (BM) 2.400 – 0.001 i (VAT)
5_AC/TiO_2	2.767 – 0.156 i (BM) 2.733 – 0.152 i (VAT)	2.465 – 0.017 i (BM) 2.438 – 0.017 i (VAT)	2.392 – 0.002 i (BM) 2.368 – 0.002 i (VAT)	2.321 – 0.002 i (BM) 2.298 – 0.003 i (VAT)
15_AC/TiO_2	2.409 – 0.144 i (BM) 2.431 – 0.118 i (VAT)	2.192 – 0.016 i (BM) 2.207 – 0.017 i (VAT)	2.137 – 0.006 i (BM) 2.151 – 0.006 i (VAT)	2.084 – 0.007 i (BM) 2.096 – 0.007 i (VAT)
30_AC/TiO_2	2.079 – 0.073 i (BM) 2.122 – 0.082 i (VAT)	1.944 – 0.015 i (BM) 1.971 – 0.016 i (VAT)	1.907 – 0.010 i (BM) 1.931 – 0.010 i (VAT)	1.870 – 0.012 i (BM) 1.891 – 0.011 i (VAT)
75_AC/TiO_2	1.615 – 0.021 i (BM) 1.644 – 0.027 i (VAT)	1.589 – 0.013 i (BM) 1.605 – 0.014 i (VAT)	1.574 – 0.015 i (BM) 1.588 – 0.015 i (VAT)	1.560 – 0.019 i (BM) 1.572 – 0.018 i (VAT)

Table 2. *AC/TiO_2 composites complex refractive indices calculated from BM and VA laws, using component (AC and TiO_2) complex refractive index extracted from [23] for TiO_2 particles and from Hota & Diaz [43] for carbon part of AC.*

The refractive index of AC, which is a porous component, were obtained using Bruggeman's mixing law for an effective medium composed of an AC skeleton with water-filled pores. The pore volume ratio of AC was fixed at 0.7, considering the effect of preparation by mechanosynthesis on pore degradation determined from previous micro-texture characterizations of the AC [35,44]. Based on equation 6, the refractive index of AC considers the refractive indices of the two components (water and carbon) as well as their respective volume fractions. Note that the complex refractive index of TiO_2 does not have an imaginary term in the visible-wavelength range (400–500 nm), indicating that the material does not absorb visible light. However, it does absorb in the UV-wavelength region, which is consistent with the semiconductor band-gap energy of ~3.0 eV for the rutile phase and 3.23 eV for anatase.

The radiative properties were defined for each AC/TiO_2 composite using the modified BHMIE program: input parameters were the complex refractive indices calculated from the VA or BM formulae (Table 2), the Gaussian parameters of the particle size distribution, and composite density (Table 1). The theoretical predictions were run for four wavelengths, i.e. 350, 400, 450, and 500 nm. Figure 4 reports the radiative properties obtained here for 6_AC/TiO_2 and 74_AC/TiO_2 composites, to compare the effect of choice of mixing law on the values of these properties.

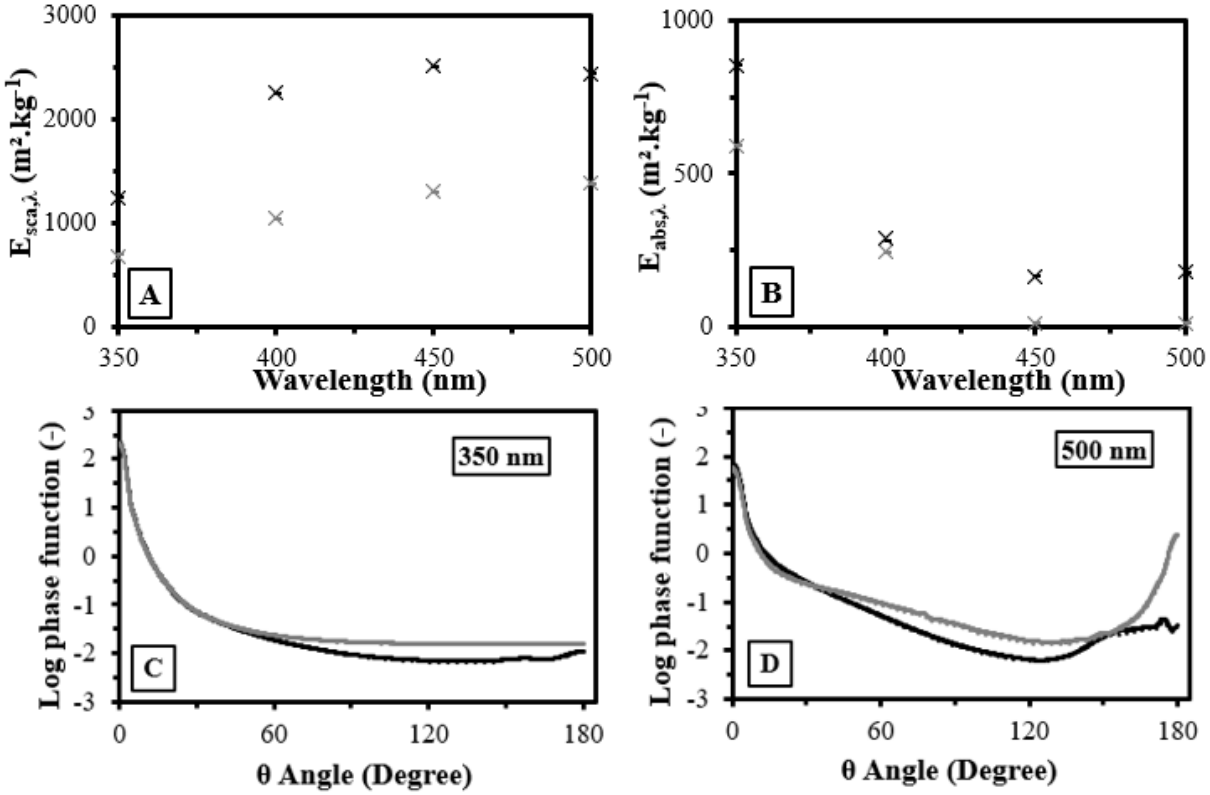

Figure 4. *Radiative properties of 6_AC/TiO_2 (grey curves and marks) 74_AC/TiO_2 composites (black curves and marks) calculated using effective AC/TiO_2 complex refractive index predicted through BM (continuous line and minus mark) and VA (dotted line and cross mark): $E_{sca,\lambda}$ (A) ; $E_{abs,\lambda}$ (B) ; and $p(\theta,\theta')$ angle-dependent scattering function at 350 nm (C) and 500 nm (D). Relative errors were lower than 10% of the indicated values for all the properties.*

The composite preparation processing conditions have been previously studied and optimized [35], showing a variability of less than 5% in the composite compositions. The errors induced by this content variability of the composites, shown in Figure 4, are derived from Equation 7 in which the composition fraction is involved twice. The results obtained were almost perfectly matched between the two mixing laws for all radiative properties. Note that this observation holds true for both the 6_AC/TiO_2 and 74_AC/TiO_2 composite materials, despite their extremely different compositional profiles. This result is consistent with previous studies that have already highlighted the closeness of predictions between VA and BM formulae for low-κ dielectric composites [39]. Moreover, Figure 4.C and 4.D allow us to assert that is strongly scattered forward by the composite particles whatever the composition. Indeed, note that there is a four order of magnitude difference between light scattered forward and through other directions.

The closeness between the two predictions highlights that the effective complex refractive index for the coupled AC/TiO_2 media studied here is almost independent of the spatial arrangement of its AC and TiO_2 subcomponents (see Figure 3). Given these results, it was decided to keep only the radiative properties predicted from BM law for the rest of the study.

The theoretically-predicted radiative properties of each AC/TiO_2 composite were validated by comparing theoretically-predicted using MCM1 against the experimentally-measured reference transmittance. For this purpose, experimental transmittance measurements were done on each AC/TiO_2 composition for different suspension concentrations using the optical bench described. Three suspension concentrations, i.e. 0.01 $kg.m^{-3}$, 0.05 $kg.m^{-3}$ and 0.1 $kg.m^{-3}$, were selected to cover a wide range of optical behaviors. The radiative properties predicted by the BM model at each of these concentrations were introduced as input parameters into MCM1 to simulate transmittance measurement through the experimental system. Figure 5 plots both the theoretical and experimental transmittance spectra.

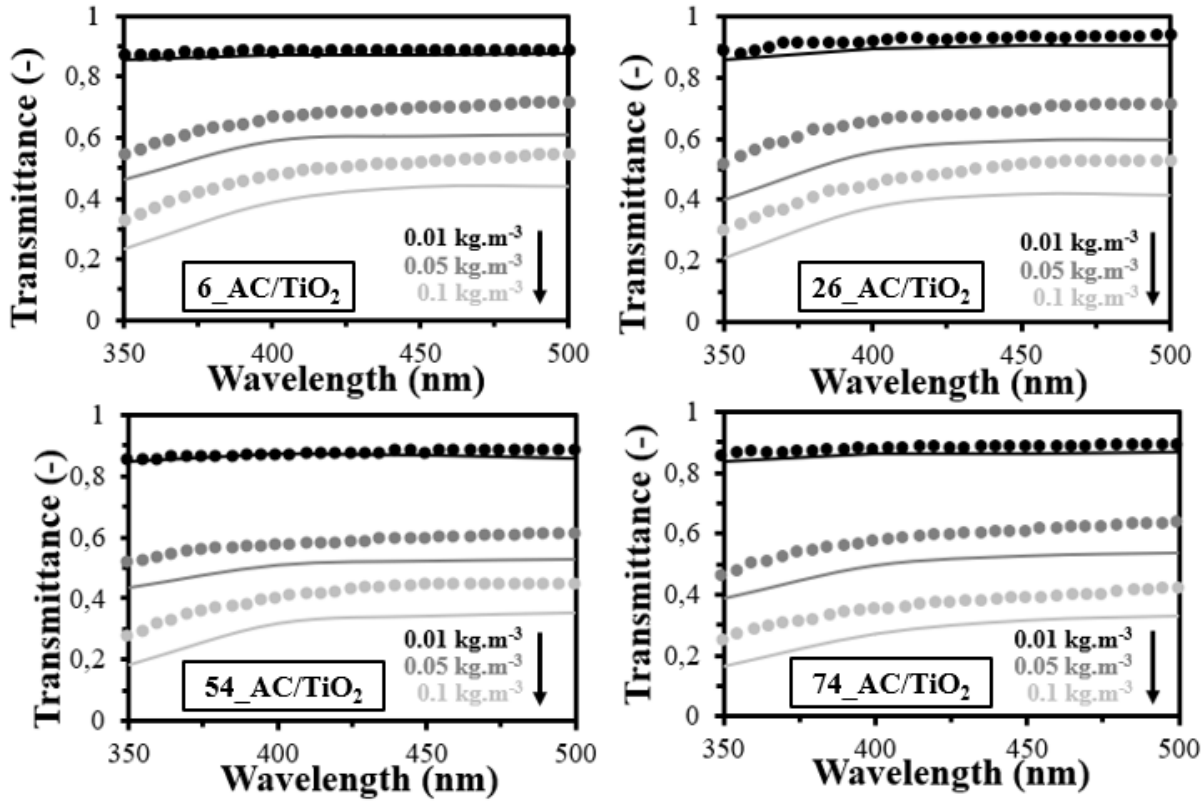

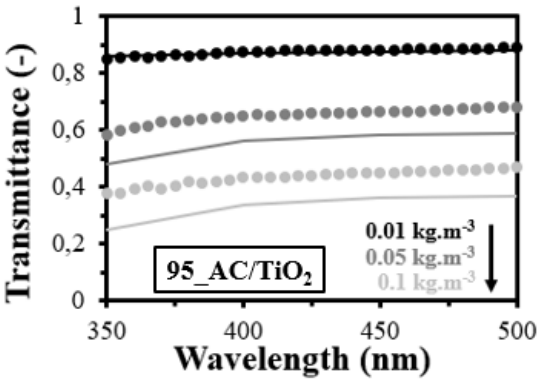

Figure 5. *Transmittance predicted (-) from BM-computed radiative properties introduced into MCM1 for three AC/TiO_2-composite suspension concentrations and for each composition (as annotated on the graphs). Comparison with experimentally-measured transmittance (○). Relative errors were lower than 4% of the displayed value for experimental transmittances and on the order of 5% for the modelled ones.*

First, it should be noted that besides the experimental uncertainties, the uncertainty related to modelled transmittance results is mainly induced by the composition variability of the prepared materials [35] and is on the order of ± 5%. Note too that, as expected, the transmittance values obtained for every composition and all wavelengths position themselves between the transmittance obtained for pure AC and pure TiO_2 (Figure S1). The experimentally-measured transmittance (Figure 5) tends to decrease as a function of particle concentration whatever the AC/TiO2 composition studied. An increase of particle concentration corresponds to an increase in number of particles per unit volume, which leads to an increase in particle–photon interactions due to the coupled phenomena of absorption and scattering. The transmittances value were very high at low concentration (0.01 $kg.m^{-3}$) for which the obtained value was about 83%. Note that for higher concentrations, the variation in transmittance differs as a function of wavelength range. In the 400–500 nm wavelength range, transmittance is found to be 40%, whereas in the 350–400 nm wavelength range, there was a much stronger decrease in transmittance, reaching a value close to 30% for some compositions. This difference between these two wavelength ranges is linked to the phenomena involved. In the visible range, absorption by AC is dominant, whereas in the UV range, absorption is strongly directed by TiO_2 behavior. These results, in agreement with the literature for suspensions of simple catalysts [23], can be explained by the effective radiative properties of the particles (Figure 4) which differ strongly between the two domains considered. For each composition, the only factor that differs between wavelengths is the complex refractive index of the AC and TiO_2

components. Thus, the highest variations in transmittance with wavelength can be attributed to the differences in complex refractive index of both AC and TiO_2 from 350 to 500 nm (Table 2).

Analysis of the influence of composition finds that transmittance varied with AC-content in the AC/TiO_2 composites. The increase in suspension concentration led to an increase in variation of transmittance as a function of composition at all wavelength ranges studied. For suspension concentrations of 0.1 kg.m^{-3}, the largest variations in transmittance were observed at 350 nm. Transmittance variations of 15 points were observed for the 74_AC/TiO_2 composition and about 5 points for the 95_AC/TiO_2 composition. The largest variation was observed for the 6_AC/TiO_2 composition for which transmittance increased from 30% at 350 nm to 55% at 500 nm. These disparities in transmittance variation as a function of wavelength and composition can also be explained by the radiative properties of the particles and their dependence on the refractive indices of the two components that make up the particles. As described in Table 2, AC and TiO_2 have very different optical properties. The variation in the effective coefficients reported in Figure 4 highlights the strong absorbing nature of AC over the whole spectral range considered, whereas TiO_2 presents two distinct behaviors—one in the visible range and another in the UV range. However, the variation in transmittance with composition for a given spectral range is linked not only to the refractive indices of the composite components but also to composite density. Note that the density of the composite (see Table 1) changes significantly between compositions, from 0.64 up to 3.7 g.cm^{-3}, which leads to an increase in the volume fraction of particles in the suspension and therefore in their specific extinction coefficients. It is likely that a decrease in complex refractive index leads to a decrease in transmittance while a decrease in density leads to an increase in transmittance.

Analysis of the theoretically-predicted transmittances in Figure 5 finds that the variations in experimental transmittance with composition and wavelength described above were correctly fitted by the theoretical curves. However, across the whole range of compositions and wavelengths, the theoretical curves are all positioned below the experimental curves. The difference between theoretical and experimental transmittance increases with concentration. Indeed, the difference between theoretical and experimental curves was about 1–3 points of transmittance value for the lowest suspension concentration, i.e. 0.01 kg.m^{-3}, but in the 8–11 points range for suspension concentrations of 0.05 and 0.1 kg.m^{-3}. For the high particle concentrations, the effective scattering coefficient $k_{sca,\lambda} = E_{sca,\lambda}.C_{susp}$ (m^{-1}) of AC/TiO_2 composites was at least 100 m^{-1} or higher. Therefore, the difference between the

theoretical and experimental transmittance curves is mainly attributed to the experimental conditions. As previously shown, for suspensions with high diffusion coefficients ($k_{sca,\lambda} = E_{sca,\lambda}.C_{susp} \approx 200$ m^{-1}), theoretical transmittance values are underestimated by 15–20 points compared to measured values [23]. In light of these considerations, we conclude that the experimental transmittance profiles are satisfactorily fitted by the proposed theoretical approach. The transmittance variations are modelled as a function of wavelength and composition taking into account the theoretically-predicted complex refractive index of the effective medium AC/TiO_2.

3.2. Radiative transfer analysis in compositionally-varied AC/TiO_2 suspensions

Recall that to describe the photo-oxidative capacities of a photo-reactor, it is necessary to establish the reaction kinetics governing the process that transforms the matter [32]. These photo-reaction kinetics will depend on the application envisaged (photo-reduction of CO_2, hydrogenation, photocatalytic oxidation of pollutants) and consequently on the coupled catalyst–indicator pairings selected [17]. However, the literature has clearly established [45,46] that they are a function of two main local quantities, i.e. the quantity of matter (concentration) and the quantity of available photons. Let us focus on this second key quantity, which is an important preliminary step towards optimizing the photo-reactor configuration, by rigorously defining the locally available radiant energy. For this purpose, simulations were carried out on a parallel-plate photoreactor in which no photoreaction takes place. In order to generalize this study, the irradiation conditions (radiant flux density) and the reactor thickness are dimensionless.

Solving the RTE, based on the MCM2 algorithm presented above, affords a one-dimensional description of the local available radiant energy, G_λ, at any wavelength in the polymethyl methacrylate measuring cell, which can be assimilated to a parallel-plate photoreactor [23]. The UV range is particularly relevant here, as it corresponds to photons with the minimum energy required to activate the TiO_2 photocatalyst . The model was then used to investigate the local available radiant energy at 350 nm, normalized from 0 to 1 considering the incident collimated density flux Φ_0 = 1 W.m^{-2}. We ran 7 simulations for two compositions, i.e. 6_AC/TiO_2 and 74_AC/TiO_2, and varying the suspension concentration as follows: 0.005, 0.020, 0.050, 0.080, 0.150, 0.300, and 0.500 kg.m^{-3} (Figure 6).

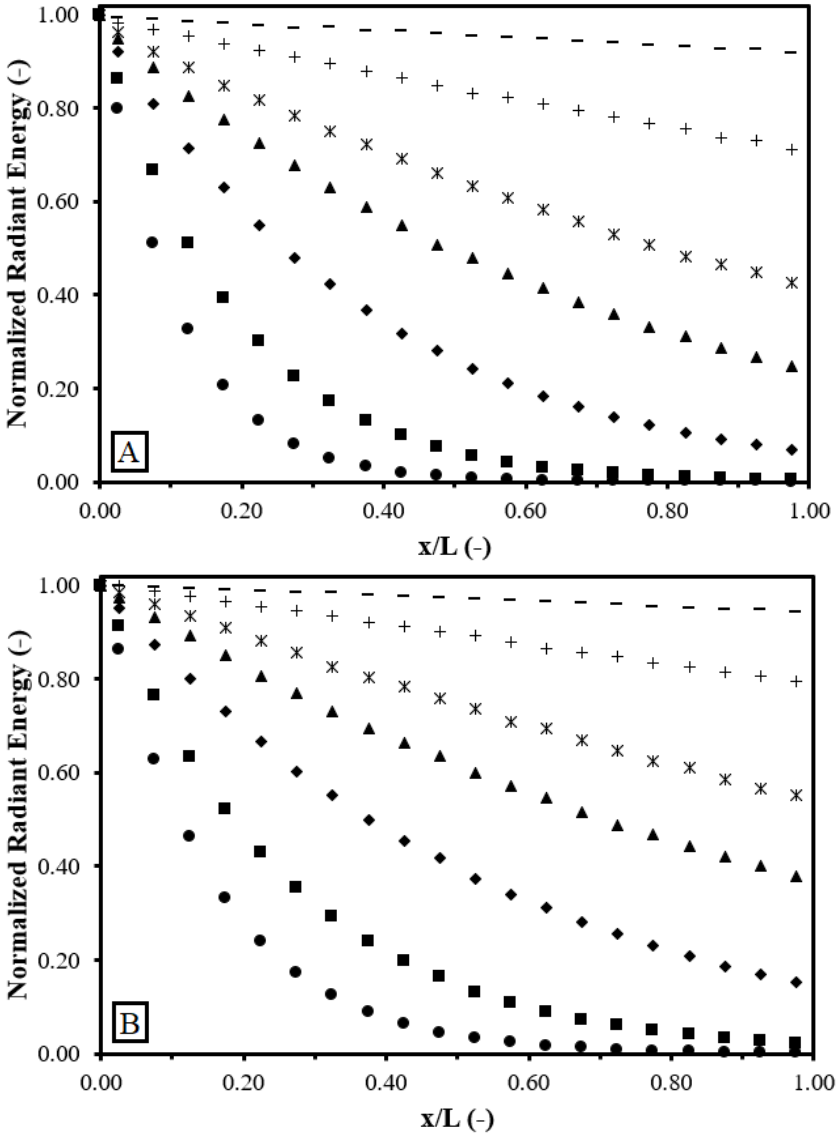

Figure 6. *Normalized local available radiant energy G(x/L) predicted at 350 nm through MCM2 using BM radiative properties predicted for several 74_AC/TiO₂ (A) and 6_AC/TiO₂ (B) composite suspension concentrations in kg.m^{-3}: 0.005 (-) ; 0.02 (+); 0.05 (*); 0.08 (▲); 0.15 (♦); 0.3 (■); 0.5 (●). The medium thickness was represented through its dimensionless x/L ratio, where L is the medium total thickness, i.e. 0.02 m. Relative errors were lower than 3% of the displayed value.*

Note that at very low suspension concentrations (0.005–0.02 kg.m^{-3}) and for both AC/TiO$_2$ compositions, the radiant energy was still very high at the exit of the photoreactor. Indeed, 80%–90% of the incident radiant energy was still available for x/L≈ 1. The concentration of AC/TiO$_2$ particles in the system was not high enough to absorb all the incident radiant energy along the thickness of the media. Obviously, then, AC/TiO$_2$ suspension concentration in this case should be increased to optimize the quantity of radiant energy

extinguished and thus used in the photoreactor. Conversely, when a high concentration is chosen, i.e. 0.5 $kg.m^{-3}$, then the extinction of light is so high that for both 74_AC/TiO_2 and 6_AC/TiO_2, there was no more radiant energy available in the photoreactor for a normalized thickness of 0.6 and 0.8, respectively. Consequently, this creates a dark zone corresponding respectively to 40% and 20% of the photoreactor volume for 74_AC/TiO_2 and 6_AC/TiO_2 composites. In this dark zone, the AC/TiO_2 photocatalyst particles are not photo-excited. The expression of the local radiant energy available at each point of the reactor then allows – for a given parallel-plate reactor thickness – to approximate the optimal composite concentration leading to the extinction of all incident photons while avoiding the creation of dark zones. Plotting the two profiles, i.e. 74_AC/TiO_2 and 6_AC/TiO_2, is sufficient to reach the approximation that the optimal concentration is around 0.15 $kg.m^{-3}$ for 74_AC/TiO_2 (Figure 6.A) and 0.3 $kg.m^{-3}$ for 6_AC/TiO_2 (Figure 6.B).

In order to move further forward in the photoreaction study, we need to evaluate the total rate of energy absorbed, which can be used to compute the number of photons available to initiate the photoexcitation The total absorbed energy inside the photoreactor $<A_\lambda>$ is introduced. This quantity necessarily intervenes in all formalisms of photoreaction kinetics to establish the capacities of the photoreactor, which are generally established for or as a function of the suspension concentration. This quantity results from integrating the local available radiant energy along the normalized photoreactor thickness [15] through Equation 8:

$$< A_\lambda > = E_{abs,\lambda} C_{susp} \int_0^L G_\lambda \, dx \qquad \text{(Equation 8)}$$

The total energy absorbed, A_λ, was calculated from the local available radiant energy profiles obtained for each studied AC/TiO_2 composition. The normalized total absorbed energy ($<A_\lambda>/A_{0,\lambda}$ where $A_{0,\lambda} = \Phi_{0,\lambda}/L$) which correspond to the total rate of energy absorbed, can then be plotted as a function of the suspension concentration.

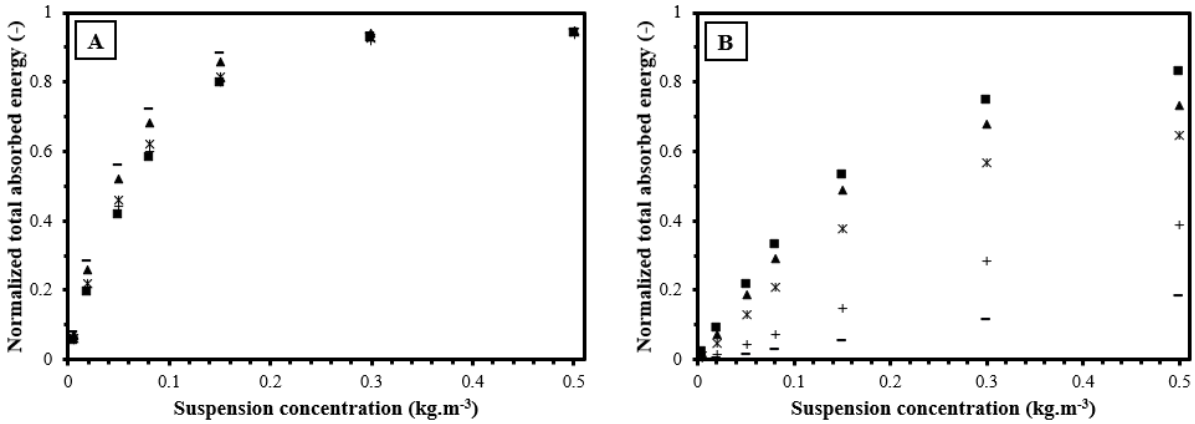

Figure 7. *Normalized absorbed energy at 350 (A) and 500 nm (B) within the measuring cell assimilated to parallel-plate-photoreactor (thickness = 0.02 m) as a function of the suspension concentration for each AC/TiO_2 studied compositions : 6_AC/TiO_2 (–) ; 26_AC/TiO_2 (+) ; 54_AC/TiO_2 (*) ; 74 AC/TiO_2 (▲) and 95_AC/TiO_2 (■).*

Note that the rate of energy absorbed at 350 nm plotted as a function the optical thickness (Figure 7.A) reached a plateau of absorbed energy for each studied AC/TiO_2 composition. The rate of energy absorbed at 350 nm in the photoreactor was found to increase with increasing suspension concentration. However, note that the curve shape is similar whatever the TiO_2 content in the AC/TiO_2 composite. To illustrate, the rate of energy absorbed at the plateau for all the AC/TiO_2 composition is 0.95. The plateau value results from two phenomena: (i) photon absorption contribute positively to the plateau value while (ii) photon scattering out from the medium contributes negatively [15].

On the other hand, at 500 nm, the rate of energy absorbed (Figure 7.B) decreases with increasing TiO_2 content in the AC/TiO_2 medium. Noted that at 500 nm and highest suspension concentration, the highest rate of energy absorbed, i.e. 0.83, was observed in the 95_AC/TiO_2 whereas the lowest rate of energy absorbed, at 0.18, was observed in the 6_AC/TiO_2 medium. Note that even at high suspension concentrations, no plateau is observed for any composition. It means that the number of particles in the medium is still to low to absorb all the entering photons or scatter them backwards to the outside of the reactor.

As stated earlier, to optimize a defined parallel-plate photoreactor (here L = 0.02 m) containing suspended medium, we first have to assess the minimum concentration required to reach the highest rate of absorbed energy. At the wavelength of interest, i.e. 350 nm (Figure 7.A), the rate of energy absorbed reach a plateau for suspension concentrations between 0.15

and 0.3 $kg.m^{-3}$. For each composition, it was chosen to interpolate the concentration value for which the rate of total absorbed energy reach 0.9. The optimal concentration values are reported in Table 3. The optimal concentration value varies weakly with an increase of TiO_2-content in the composites.

	Units	95_AC/TiO_2	74_AC/TiO_2	54_AC/TiO_2	26_AC/TiO_2	6_AC/TiO_2
$C_{optimal}$	$\times 10^{-1}$ $kg.m^{-3}$	2.74	2.31	2.69	2.82	2.00
r_{TiO2}	-	0.19	0.31	0.37	0.63	0.83

Table 3. *Summary of each AC/TiO_2 composite optimal concentration for maximizing radiant energy use in the studied photoreactor. Total absorbed energy rate at 350 nm by the TiO_2 component estimated for each AC/TiO_2 composition.*

The rate of energy absorbed at 500 nm (Figure 7.B) can be attributed to the behavior of AC, which is the only component driving absorption, while TiO_2 absorption is null at this wavelength. The AC component also exhibits an almost invariant complex refractive index across wavelengths (Table 2). We thus assumed that the rate of energy absorbed by AC at 350 nm for each AC/TiO_2 composition and suspension concentration is the same as total rate of energy absorbed at the same composition and concentration in Figure 7.B, that was attributed to AC only. Working to this assumption made it possible to evaluate, at 350 nm, the rate of energy absorbed by TiO_2, which is the component of interest driving the photocatalytic reaction. We evaluated this rate, called r_{TiO2}, by subtracting the total energy rate observed at 500 nm and optimal concentration from the total energy rate obtained at 350 nm and optimal concentration for each AC/TiO_2 composition. The results are summarized in Table 3.

r_{TiO2} vary considerably with TiO_2-content in AC/TiO_2 composites. Indeed, r_{TiO2} was highest for the 6_AC/TiO_2 composite (r_{TiO2}=0.83) but fell by 46%, i.e. r_{TiO2}=0.37, when TiO_2 content was almost halved (54_AC/TiO_2). When TiO_2 content was reduced to under 25%, r_{TiO2} values fell from 0.31 for 74_AC/TiO_2 to 0.19 for 95_AC/TiO_2. As expected, photocatalytic applications would gain from using high-TiO_2-content suspensions, i.e. the 6_AC/TiO_2–54_AC/TiO_2 composites here, to maximize the quantity of photons effectively used by the photoreactor medium for photo-oxidation.

Finally, two key information emerge from this approach. First, the optimal concentrations of composite suspensions are very close and are almost independent of the AC/TiO_2 composition of the composite. This suggests that the amount of radiation consumed is identical regardless of the composition. The second point concerns the use of absorbed radiation. The results reported in Table 3 clearly show that the number of photons effectively absorbed by the catalyst is dependent on the proportion of TiO2 in the composite. These results are consistent with expectations, but have now been demonstrated, and emphasize the problem of solar radiation management. There is the need to design a composite with an adsorbent to ensure a storage function and TiO_2 at a high rate to initiate the photo-excitation process. These components have antagonistic characteristics to optimize both the use of radiation and the storage function.

Conclusion

The purpose of this work as to evaluate photon availability for photo-oxidation in a parallel-plate photoreactor containing a broad range of compositionally-varied AC/TiO_2 composite particulate media. We employed a theoretical approach coupled to experimental validation to define the radiative properties of the AC/TiO_2 composites, as these properties are key for analyzing how photons get scattered and absorbed from the time they enter the photoreactor. A classical theoretical approach validated by experimental results has been applied to original composite materials whose properties seem relevant to ensure an optimal management of the solar resource by ensuring a double functionality of storage and photoexcitation.

The key point is the use of the Monte Carlo algorithm to predict the local radiant energy available through a parallel plate photoreactor as a function of suspension concentration for each AC/TiO_2 composition. Simulations were conducted for all composite compositions developed at different particle concentrations. A first result, in agreement with studies conducted in the literature, confirms that the locally available radiant energy varies strongly with the particle concentration. The attention was then focused on the effect of the AC/TiO_2 composition. For this purpose, the locally absorbed radiant energy was determined in order to evaluate the amount of photons effectively available for photo-excitation with respect to the amount absorbed by the adsorbent material. On the one hand, it is found that the volume fraction of particles leading to the total absorption of radiation varies very little from one composition

to another. Thus, the composites, whatever their composition, absorb almost the same quantity of photons whether they are intended to be absorbed by the catalyst to initiate the photo-excitation process or lost due to their absorption by the adsorbent material. The attention was then focused on the amount of photons absorbed as an efficient manner by the catalyst which increases directly with the catalyst content in the composite. We show that it is possible to assess the radiant energy effectively absorbed by the TiO_2 component, which is the component that drives photocatalytic oxidation in water treatment applications. This novel result highlighted the benefit of working with medium-to-high TiO_2-content (50%–90%v) AC/TiO_2 compositions in order to maximize the number of photons effectively used for photo-excitation. Note that in these compositions, the suspensions are photocatalytically 'operational' but are still not efficient. It also highlighted that for low-TiO_2-content materials, the number of photons available for photo-oxidation is very low due to the stochastic structure of the AC/TiO_2 composite.

This key result also reveals a need to structurally arrange the AC/TiO_2 composites. As a matter of fact, this study clearly emphasizes the problem of elaboration of composite able to manage the use of the solar resource by proposing a functionality of storage by adsorbing materials while preserving an optimal use of the radiation by the catalyst. It is shown that, due to the antagonistic optical properties of the two components, the presence of the AC affects very significantly the amount of photons available to initiate the photo-excitation. In order to optimize the performance of the composites for a solar application, a first solution consists in selecting the composite with a composition allowing the best compromise between the two functionalities sought. But more recently, research is being carried out on the synthesis of AC/TiO_2 composites with a core-shell structure in order to spatially organize the material within the composite in a way that is beneficial for photon absorption. The aim is to control the distribution of the components by favoring the presence of the catalyst on the surface and the adsorbent material in the volume while preserving its adsorption capacity.

Acknowledgements

This work was supported by the Occitanie Region in France and by European Regional Development Fund (ERDF) n° 201700167402 provided by the European Union.

References

[1] Herrmann J-M., 1995, "Heterogenous photocatalysis : an emerging discipline involving multiphase systems", Cat. Today 24, 157-164.

[2] Malato S., Blanco J., Vidal A., Richter C., 2002, "Photocatalysis with solar energy at a pilot-plant scale: An overview", Appl. Cat. B: Environ. 37 (1), 1-15.

[3] Chekir N., Boukendakdji H., Igoud S., Taane W., 2012, "Solar energy for the benefit of water treatment: Solar photoreactor", Proced. Eng. 33, 174-180.

[4] Plantard G., Azais A., Mendret J., Brosillon S., Goetz V., 2018, "Coupling of photocatalytic and separation processes as a contribution to mineralization of wastewater", Chemical Eng. And Processing: Process intensification 134, 115-123.

[5] Castellanos R.M., Bassin J.P., Dezotti M., Boaventura R.A.R., Vilar V.J.P., 2020, "Tub-in-tube membrane reactor for heterogeneous TiO_2 photocatalysis with radial addition of H2O2." Chemical Engineering Journal 395, 124998.

[6] Yoneyama H., Sakamoto H., Tamura H., 1975, "A photo-electrochemical cell with production of hydrogen and oxygen by a cell reaction", Electrochim. Act. 20, 341-345.

[7] Khan S.U.M., Al-Shahry M., Ingler W.B.J., 2002, "Efficient photochemical water splitting by a chemically modified n-TiO_2", Science 297, 2243-2245.

[8] Wu J.C.S., Lin H-M., Lai C-L., 2005, "Photo reduction of CO_2 to methanol using optical-fiber photoreactor", Appl. Cat. A: Gen. 296 (2), 194-200.

[9] Nguyen V-H., Wu J.C.S, Chiou C-H., 2008, "Photoreduction of CO_2 over Ruthenium dye-sensitized TiO_2-based catalysts under concentrated natural sunlight", Cat. Comm. 9 (10), 2073-2076.

[10] Alfano O.M., Romero R.L., Cassano A.E., 1986, "Radiation field modelling in photoreactors – I. Homogeneous media", Chem. Eng. Sci. 41 (3), 421-444.

[11] Ješić D., Jurković D.L., Pohar A., Suhadolnik L., Likozar B., 2021, "Engineering photocatalytic and photoelectrocatalytic CO_2 reduction reactions: Mechanisms, intrinsic kinetics, mass transfer resistances, reactors and multi-scale modelling simulations", Chem. Eng. J. 407, 126799.

[12] Reddy P.A.K., Reddy P.V.L., Kwon E., Kim K.H., Akter T., Kalagara S., 2016, "Recent advances in photocatalytic treatment of pollutants in aqueous media", Environ. Int. 91, 94-103.

[13] Long Z., Li Q., Wei T., Zhang G., Ren Z., 2020, "Historical development and prospects of photocatalysts for pollutant removal in water" J. of Haz. Mat. 395, 122599.

[14] Alfano O.M., Romero R.L., Cassano A.E., 1986, "Radiation field modelling in photoreactors – II. Heterogeneous media", Chem. Eng. Sci. 41 (5), 1137-1153.

[15] Cornet J.F., Dussap C.G., Dubertret G., 1992, "A structured model for simulation of cultures of the cyanobacterium *spirulina platensis* in photobioreactors: I. coupling between light transfer and growth kinetics", Biotechn. & Bioeng. 40, 817-825.

[16] Huang Q., Liu T., Yang J., Yao L., Gao L., 2011, "Evaluation of radiative transfer using the finite volume method in cylindrical photoreactors", Chem. Eng. Sci. 66 (17), 3930-3940.

[17] Supplis C., Gros F., Dahi G., Dauchet J., Roudet M., Gloaguen F., Cornet J-F., 2018, "Spectral radiative analysis of bio-inspired H_2 production in a benchmark photoreactor: A first investigation using spatial photonic balance", Int. J. of Hydr. Ener. 43 (17), 8221-8231.

[18] Doicu A., Mishchenko M.I., Trautmann T., 2020, "Electromagnetic scattering by discrete random media illuminated by a Gaussian beam II: Solution of the radiative transfer equation", J. of Quant. Spectr. & Rad. Trans. 256, 107297.

[19] Rochatte V., Dahi G., Eskandari A., Dauchet J., Gros F., Roudet M., Cornet J-F., 2017, "Radiative transfer approach using Monte Carlo Method for actinometry in complex geometry and its application to Reinecke salt photodissociation within innovative pilot-scale photo(bio)reactors", Chem. Eng. J. 308, 940-953.

[20] Menbari A., Alemrajabi A.A., Rezaei A., 2016, "Heat transfer analysis and the effect of CuO/Water nanofluid on direct absorption concentrating solar collector", Appl. Therm. Eng. 104, 176-183.

[21] Mie G., 1908, "Beitrage zur Optik truber Medien, speziell kolloidaler metallosungen", Annalen der physik 25, 377-445. http://dx.doi.org/10.1002/andp.19083300302

[22] Caldas M., Semião V., 1999, "Modelling of scattering and absorption coefficients for a polydispersion", Inter. J. of Heat & Mass Trans. 42 (24), 4535-4548.

[23] Ribeiro E., Plantard G., Cornet J-F., Gros F., Caliot C., Goetz V., 2021, "Experimental and theoretical coupled approaches for the analysis of radiative transfer in photoreactors containing particulate media: case study of TiO_2 powders for photocatalytic reactions", Chem. Eng. Sci. 243, 116733.

[24] Galvez J., Malato S., 2003, "Solar Detoxification", United Nations Educational, Scientific and Cultural Organization.

[25] Janin T., Goetz V., Brosillon S., Plantard G., 2013, "Solar photocatalytic mineralization of 2,4-dichlorophenol and mixtures of pesticides: Kinetic model of mineralization", Solar Energy 87, 127-135.

[26] Malato S., Blanco J., Maldonado M.I., Oller I., Gernjak W., Perez-Estrada L., 2007, "Coupling solar photo-fenton and biotreatment at industrial scale: Main results of a demonstration plant", J. of Haz. Mat. 146 (3), 440-446.

[27] Puma G.L., Bono A., Krishnaiah D., Collin J.G., 2008, "Preparation of titanium dioxide photocatalyst loaded onto activated carbon support using chemical vapor deposition: A review paper", J. Haz. Mat. 157 (2-3), 209-219.

[28] Al-Mamun M.R., Kader S., Islam M.S., Khan M.Z.H., 2019, "Photocatalytic activity improvement and application of UV-TiO2 photocatalysis in textile wastewater treatment: A review", Journal of Environmental Chemical Engineering 7 (5), 103248.

[29] Wetchakun K., Wetchakun N., Sakulsermsuk S., 2019, "An overview of solar/visible light-driven heterogeneous photocatalysis for water purification: TiO_2- and ZnO based photocatalysts used in suspension photoreactors.

[30] Matos J., Laine J., Herrmann J-M., 1998, "Synergy effect in the photocatalytic degradation of phenol on a suspended mixture of titania and activated carbon" Appl. Cat. B: Environ. 18, 281-291.

[31] Alves N.S.E., Civdanes L.S., Moreira Bastos Campos T., Rossi Canuto de Menezes B., Sales Brito F., Patrocinio T., 2016, "Carbon and TiO_2 synergistic effect on methylene blue adsorption", Materials Chemistry & Physics 177, 330-338.

[32] Ribeiro E., Plantard G., Goetz V., 2021 , "TiO_2 grafted Activated Carbon elaboration by milling: composition effect on sorption and photocatalytic properties", J. of Photochem. & Photobiol. A: Chem. 408, 113108.

[33] Chekem T.C., Goetz V., Richardson Y., Plantard G., Blin J., 2019, "Modeling of adsorption/photodegradation phenomena on CA-TiO_2 composites catalyst for water detoxification", Catalysis Today 328, 183-188.

[34] Chekem T.C., Richardson Y., Drobeck M., Plantard G., Blin J., Goetz V., 2017, "Effective coupling of phenol adsorption and photodegradation at the surface of micro and mesoporous TiO_2 activated carbon", Reaction Kinetics, Mechanisms and Catalysis 122 (2), 1297-1321.

[35] Ribeiro E., Plantard G., Teyssandier F., Maury F., Sadiki N., Chaumont D., Goetz V., 2020, "Activated-Carbon/TiO_2 composites preparation: An original grafting by milling approach for solar water treatment applications", Journal of Environmental Chemical Engineering 8 (5), 104115.

[36]Matos J., Laine J., Herrmann J.M., Uzcategui D., Brito J.L., 2007, "Influence of activated carbon upon titania on aqueous photocatalytic consecutive runs of phenol photodegradation", Applied Catalysis B: Environmental 70, 461–469.

[37] Bohren C.F., Huffman D.R., 1983, "Absorption and scattering of light by small particles", John Wiley and Sons, New York.

[38] Markel V., 2016, "Introduction to the Maxwell Garnett approximation: tutorial", Journal of the Optical Society Of America A 33 (7), 1244-1256.

[39] Braun M.M., Pilon L., 2006, "Effective optical properties of non-absorbing nanoporous thin films", Thin Solid Films 496, 505-514.

[40] Maxwell Garnett J.C., 1904, "XII. Colours in metal glasses and in metallic films", Phil. Trans. of the Roy. Soc. A: Math., Phys. & Eng. Sci. 203 (359-371), 385-420.

[41] Bruggeman D.A.G., 1935, "Berechnung verschiedener physikalischer konstanten von heterogen substanzen", Ann. Phys. 24, 636-679.

[42] Sharma S., Patel P.B., Patel R.S., Vora J.J., 2007, "Density and comparative refractive index study on mixing properties of binary liquid mixtures of eucalyptol with hydrocarbons at 303.15, 308.15 and 313.15K", E-Journal of Chem. 4 (3), 343-349.

[43] Hota S.K., Diaz G., 2021, "Influence of optical constants in carbon-based dispersions for enhanced solar evaporation", J. of Therm. Anal. & Calor. 144, 741-750.

[44] Plantard G., Goetz V., Py X., 2010, "A direct method for porous particle density characterization applied to activated carbons", Adv. Powd. Technol. 21 (6), 592-598.

[45] Emeline A.V., Ryabchuk V., Serpone N., 2000, "Factors affecting the efficiency of a photocatalysed process in aqueous metal-oxide dispersions. Prospect of distinguishing between two kinetic models", J. of Photochem. & Photobiol. A: Chem. 133, 89-97.

[46] Plantard G., Janin T., Goetz V., Brosillon S., 2012, "Solar photocatalysis treatment of phytosanitary refuses: Efficiency of industrial photocatalysts", Applied Catalysis B: Environmental 115-116, 38-44.